Chemical Engineering Journal 471 (2023) 144752

Contents lists available at ScienceDirect

Chemical Engineering Journal

journal homepage: www.elsevier.com/locate/cej

One-step preparation of robust elastic plastic polyvinyl chloride sponges with a layered structure for highly efficient separation of water-in-oil emulsions

Daning Lang [a], Gang Liu [a], Ronglan Wu [a,*], Guohao Chen [a], Chengbo Zhang [a], Chao Yang [a], Wei Wang [b,c,*], Jide Wang [a], Jihong Fu [a]

[a] Key Laboratory of Oil & Gas Fine Chemicals, School of Chemical Engineering, Xinjiang University, Urumqi 830046, China
[b] Institute of Chemistry, University of Bergen, Bergen 5004, Norway
[c] Center for Pharmacy, University of Bergen, Bergen 5020, Norway

ARTICLE INFO

Keywords:
PVC food wrap
Plastic
Sponge
Elastic
Emulsions separation

ABSTRACT

To address the environmental pollution and human health issues caused by oily wastewater and PVC plastic waste, a practical zero-waste solution has been developed. In this study, PVC sponges with superlipophilic and superhydrophobic properties were prepared using vapor induced phase inversion and recycling PVC food wrap, without the use of any additives. This sponge effectively separates oil and water. The pore size of PVC sponges could be adjusted by varying the PVC concentration and solvent ratio, which led to improvements in pore density, specific surface area, porosity, oil sorption capacity, and emulsion separation performance. The emulsion separation experiment demonstrated that the 7 wt% PVC sponge (7-0-1) can efficiently separate oil from water-in-oil emulsion, with excellent separation efficiency and a flux of 161.5 $L{\cdot}m^{-2}{\cdot}h^{-1}{\cdot}bar^{-1}$. Moreover, the sponge exhibits impressive properties such as elastic recovery, flexibility, self-cleaning, and mechanical strength. Remarkably, even after recycling, the sponge maintains its hydrophobicity and emulsion separation performance. This hydrophobic sponge has great potential for mass production and oil–water separation such as in oil spill accidents.

1. Introduction

Oily wastewater treatment has become a critical environmental concern owing to oil spills, as well as the discharge of organic pollutants and petroleum wastewater from industries. This pollution inflicts severe harm on marine ecosystems, the environment, and human health [1,2]. In response, several studies have focused on isolating oil pollutants, organic pollutants, and emulsions from water [3–5].

Porous materials have taken the lead as a remarkable category of separation materials, finding extensive application in the retrieval and partitioning of crude oil [6,7], organic reagent [8] and emulsion [9,10], eclipsing metal mesh [11,12], composite membrane [13], and functional particle materials [14–16] due to their unique three-dimensional network structure, impressive adsorption capacity, lightweight nature, and outstanding compression capabilities. For example, Wang et al. have demonstrated the efficacy of a novel silica aerogel membrane with a mesoporous structure and superhydrophobicity of 161° prepared via the sol–gel method. This aerogel membrane boasts a separation efficiency exceeding 99.9% for surfactant-stabilized water-in-oil (w/o) emulsions [17]. Wang and Weng developed a methodology for fabricating polyacrylonitrile fiber/graphene oxide (PAN/RGO) composite porous materials. By ingeniously merging hydrothermal reactions and freeze-drying techniques, they utilized the potential of discarded polyacrylonitrile fiber (PAN) alongside the dynamic properties of graphene oxide (RGO) as the elemental building blocks [18]. While numerous reports on porous materials have surfaced, encompassing biomass aerogels [19,20], polymer sponges [21] and composite materials [22], several limitations have impeded their practical application and mass production. These shortcomings primarily come from convoluted preparation processes and unsatisfactory elasticity. Such predicaments restrict their potential in real-world scenarios and large-scale manufacturing endeavors. There is, therefore, an exigent need for porous materials that offer straightforward preparation, economical raw materials, and emulsion separation capabilities.

* Corresponding authors at: Institute of Chemistry, University of Bergen, Bergen 5004, Norway.
E-mail addresses: wuronglan@163.com (R. Wu), wei.wang@uib.no (W. Wang).

https://doi.org/10.1016/j.cej.2023.144752
Received 28 April 2023; Received in revised form 14 June 2023; Accepted 10 July 2023
Available online 14 July 2023

Apart from the environmental threat of oil pollution, the recycling and treatment of waste plastics constitute another significant challenge [23,24]. Plastics, especially polyvinyl chloride (PVC), exhibit remarkable resistance to water, acid, alkali, and chemical corrosion, making them ubiquitous in food, packaging, construction, and other industries [25,26]. Unfortunately, PVC is inherently unstable when subjected to high temperatures and prolonged exposure to light, leading to its decomposition and the release of hydrogen chloride, which is harmful to human health [27]. Moreover, the fragments of decomposed PVC remain in the soil and rivers, threatening the survival of aquatic plants and animals [28]. Given the ubiquity of PVC in everyday life and the resulting production of waste PVC plastics, there is an urgent need to address the resultant "white pollution" problems. Recycling PVC plastics provides an effective solution to reduce environmental pollution, minimize the secondary pollution caused by landfill and incineration of waste plastics, and realize resource utilization. At the same time, compared with the novel separator skimmer [29], the technology that can effectively recycle PVC plastic and prepare the separated material is more economical and easier to realize the actual industrial production.

After a comprehensive literature review, it was determined that materials capable of emulsion separation exhibit at least one of two fundamental characteristics [30]: (1) a unique micro-nanostructured surface that breaks the emulsion and facilitates separation [31,32], or (2) a distinct internal pore structure that under the influence of gravity or an external force enables the emulsion to break, allowing one phase to pass through while the other is retained in the material's surface or pores [33,34].

Yang et al. investigated the separation mechanism of a sodium alginate/graphene oxide/silica aerogel (SA/GO/SiO_2-M) for w/o emulsions. They discovered that the SA/GO/SiO_2-M aerogel possesses a zigzag porous structure with superhydrophobic/superlipophilic characteristics. This enables the aerogel to filter the oil phase through an interconnected microchannel, while water droplets are blocked on the surface. Water droplets coalesce to form larger drops, resulting in droplets significantly larger than the aerogel's pore size, enabling efficient demulsification and separation [35].

Despite the excellent water and chemical resistance properties of PVC food wrap, its limited solubility in water and inadequate shareability for porous material direct production hinders its utilization in oil/water separation applications. Additionally, there are limited reports on hydrophobic PVC materials. Therefore, a novel approach is proposed that involves dissolving hydrophobic PVC materials in a suitable solvent and regenerating them through a water bath to construct a specialized porous material with emulsion separation capability. To the best of our knowledge, the development of PVC sponges from PVC food wrap has yet to be reported.

This study successfully transformed PVC food wrap into PVC sponges, which were employed for oil–water and emulsion separation. The raw material was subjected to a vapor induced phase inversion process to create a shape-controllable, superhydrophobic porous material with efficient oil sorption, emulsion separation, and reusability. The morphology, structure, and properties of the sponges were comprehensively analyzed, including their oil–water separation performance, emulsion separation performance, mechanical performance, and recycling performance. The potential applications of PVC sponges in high-value engineerings, such as oil spill treatment and oil–water separation, were also discussed. By developing PVC sponges, this study not only upcycles PVC as a valuable material but also expands its potential value.

2. Experimental section

2.1. Materials

Polyvinyl chloride (PVC) food wrap, 10 μm thick, was obtained from Nanjing Yuehuo Household Articles Co., Ltd. N,N-Dimethyloctanamide (DMF, ≥ 99.5%), and N,N-Dimethylacetamideand (DMAC, ≥ 99.5%) were purchased from Tianjin Xinbote Chemical Co., Ltd. Petroleum ether (≥98%), copper sulfate solution ($CuSO_4$, ≥ 99%), sodium chloride (NaCl, ≥ 99%), and potassium chloride (KCl, ≥ 99%) were purchased from Tianjin Yongsheng Fine Chemicals Co., Ltd. n-Hexane and n-heptane (≥98%) were purchased from China Pharmaceutical Corporation Beijing Co., silicone oil from Sigma-Aldrich, and diesel from Sichuan Chehao Trading Co., Ltd. Cyclohexane (≥99.5%) was purchased from Tianjin Fuyu Fine Chemicals Co., Ltd. All the water used in the experiment was deionized. The chemicals and reagents used in this experiment were not subjected to any further purification.

2.2. Preparation of PVC sponges

Fig. 1a presents the flow chart for the preparation of PVC sponges, which involves the following steps: first, the PVC food wrap is cut up, and then PVC solutions with concentrations of 5, 6, 7, 8, and 9 wt% are prepared by mixing DMF and DMAC solutions in different volume ratios (DMF/DMAC score of 1/0, 1/1, 1/2, 1/4, and 0/1, respectively) using magnetic stirring. Next, 5 mL of the PVC solution is transferred to a glass petri dish with a diameter of 40 mm and a height of 10 mm. The mold containing PVC solution is then placed in a 180 mm dryer for 12 h, in a container containing saturated $CuSO_4$ (98% relative humidity). To compare the oil–water separation performance and hydrophobic angle of PVC sponges, saturated NaCl (76% relative humidity) and KCl (86% relative humidity) solutions are used. Once the water vapor-induced phase inversion is complete, the obtained PVC hydrogels are soaked in water for 1 day, with the water being changed every 4 h. Finally, the PVC sponges are obtained by refrigeration and freeze-drying. The abbreviations used to represent the PVC sponges prepared in this paper are as follows: for example, 7-0-1 indicates that the sponge is prepared using a PVC concentration of 7 wt% and a DMF/DMAC volume ratio of 0/1. Unless otherwise specified, PVC sponges are prepared using saturated $CuSO_4$. Additionally, 10 wt% PVC sponges are prepared using the same procedure described above; however, these samples are not analyzed because none of the 10 wt% PVC sponges pass the w/o emulsion test.

Fig. 1b shows the experimental process involved in the preparation of PVC sponges. As can be seen from the picture, the colorless PVC solution turns into a white hydrogel after vapor deposition and induction by water vapor replacement, with a slight reduction in volume. After freeze-drying, a white PVC sponge is formed.

2.3. Preparation of recycled PVC sponges

For instance, the 7-0-1 was used in this study. The previously utilized PVC sponges were dried in an 80 °C oven for 6 h and subsequently cut into pieces to replace the PVC food wrap. The recycled PVC sponges were produced in the same manner as the original PVC sponges.

2.4. Density and porosity of PVC sponges

The density (ρ_s) of PVC is 1.4 g/cm^3, determined by the thickness and weight of the PVC food wrap. The density (ρ, g/cm^3), and porosity (P, %) of PVC sponges were calculated using Eq. (1) and Eq. (2) [36]:

$$\rho = \frac{m}{V} \tag{1}$$

$$P(\%) = \left(1 - \frac{\rho}{\rho_s}\right) \times 100\% \tag{2}$$

where m (g) and V (cm^3) are the weight and volume of PVC sponges, respectively.

2.5. Oil sorption and oil/water separation testing of PVC sponges

During a typical sorption test, the PVC sponge was immersed in a

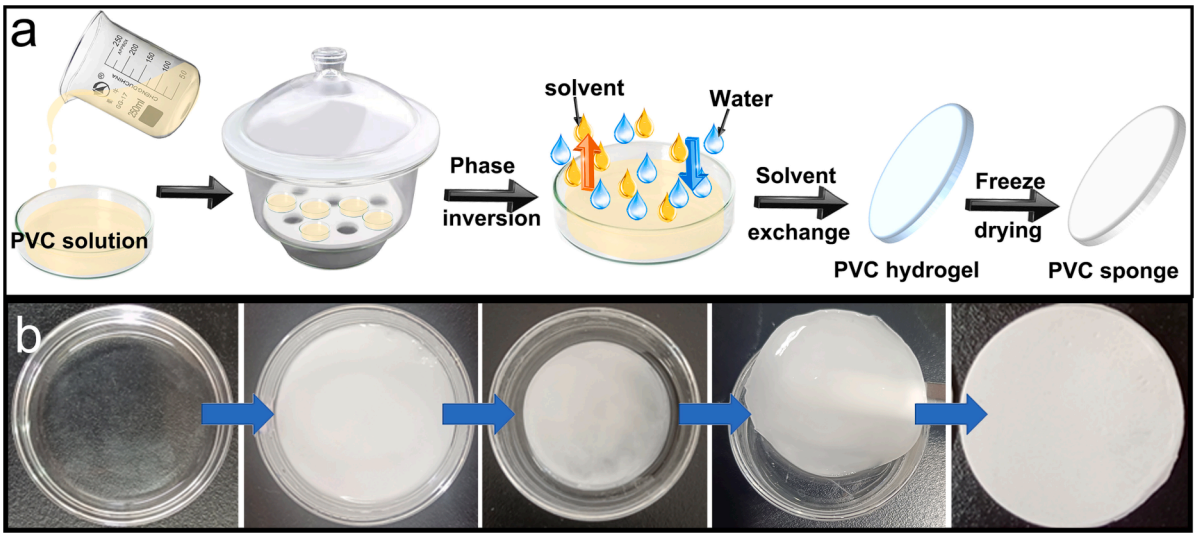

Fig. 1. (a) Schematic illustration of the synthetic procedure of the PVC sponges; (b) Photos taken during the synthetic process of the PVC sponges.

mixture of oil and water that had been dyed with oil red and methylene blue, respectively. After reaching adsorption and saturation, the PVC sponge was removed and weighed to determine its saturated mass. The adsorption capacity (Q, g/g) was then calculated using Equation (3):

$$Q = \frac{m_2 - m_1}{m_1} \tag{3}$$

where m_1 (g) and m_2 (g) represent the total mass of the sponges before and after oil sorption, respectively.

2.6. Separation performance evaluation of water-in-oil emulsions of PVC sponges

The w/o emulsions were prepared by adding 1 mL of deionized water and 0.25 g of surfactant Span 80 to 100 mL of various oils (n-hexane, cyclohexane, n-heptane, and petroleum ether). The mixture was sonicated for 1 h in a bath sonicator, followed by vigorous magnetic stirring for 3 h. The separation performance of PVC sponges for the different emulsions was evaluated using a self-made filtration device (see Fig. S1), and the flux (F, $L{\cdot}m^{-2}{\cdot}h^{-1}{\cdot}bar^{-1}$) of PVC sponges was calculated using Poiseuille's Law (Eq. 4) [37,38]. For each separation process, 5 mL of the w/o emulsion was poured onto pre-wetted PVC sponges driven by an SHB-III circulating water multi-purpose vacuum pump.

$$F = \frac{4V}{\pi d^2 \Delta t \Delta P} \tag{4}$$

where V (L), d (m), Δt (h) and ΔP (bar) represent the emulsion volume, effective diameter, passing time of PVC sponges, and additional pressure, respectively.

2.7. Testing of oil sorption cycle and emulsion separation cycle of PVC sponges

To conduct the oil absorption cycle test of the PVC sponge, the sponge is immersed in oil until it reaches adsorption saturation. The adsorption capacity is then calculated using the weighing method. The sponge is then dried at room temperature for the next cycle of adsorption, and this cycle is repeated 10 times.

In the w/o (n-hexane) emulsion separation cycle test of the PVC sponge, the sponge is placed into a self-made separation device. The time taken by the 7-0-1 to separate a 5 mL n-hexane emulsion under external force is recorded, and the n-hexane flux is calculated using Poiseuille's Law Eq. (4). The PVC sponges are then removed and dried at room temperature for the next cycle of the test. This cycle is repeated 5 times.

2.8. Instrumentation

Chemical properties were determined using fourier transform infrared spectroscopy (FTIR; VERTEX 70, Bruker, Germany) over the wavenumber range of 500–4000 cm^{-1}. The specific surface area and pore size were analyzed by Brunauer-Emmett-Teller (BET; Quantachrome-EVO, America). Surface morphology was observed using scanning electron microscopy (SEM; Zeiss sigma 300, Germany). Thermal stabilities were evaluated via thermal gravimetric analysis (TG; TGA 550, America) in the temperature range of 30–600 °C, with a temperature rate of 10 °C/min, and samples in N_2 atmosphere. Heat-release characteristics and glass transition temperature (Tg) were determined by differential scanning calorimeter (DSC; DSC Q2000, TA, America), conducted from 25 °C to 220 °C under N_2 flow of 50 mL/min, with a heating rate of 10 °C/min.

Air wettability was characterized by measuring the water contact angle (WCA) and oil contact angle (OCA) using a contact angle instrument (JJ2000B, Zhongchen, Shanghai, China). The elastic resistance of sponges (20 mm in length and 6 mm in width) was measured using a T-Series materials testing machine (H5K-T, Tinius Olsen, America) at a drawing speed of 50 mm/min. Droplet sizes of emulsions were determined using a nanometer particle potentiometer (Nano ZS90, Malvern, America). Viscoelastic properties were measured using a dynamic mechanical thermal analyzer (DMA; DMA Q800, TA, America), while the modulus and machining performance of the samples were tested using a rotational rheometer (TA DHR-1, TA, America).

3. Results and discussion

The pore sizes of sponges are closely related to their preparation parameters, particularly the solvent and PVC concentration. Fig. 2 illustrates the significant influence of the PVC concentration on the diameter, thickness, quality, density, and porosity of PVC sponges. Conversely, the DMAC/DMF solvent ratio, although intriguing, does not appear to exert a substantial impact at lower concentrations, yet manifests a significant influence at higher concentrations.

The diameter (Fig. 2a) and thickness (Fig. 2b) of sponges decrease with an increase in the PVC concentration, which is also evident from the photos in Fig. 2c. Conversely, the quality (Fig. 2d) and density (Fig. 2e) of the sponge increase with the increase in PVC concentration, while the porosity decreases (Fig. 2f). Additionally, the hardness of the

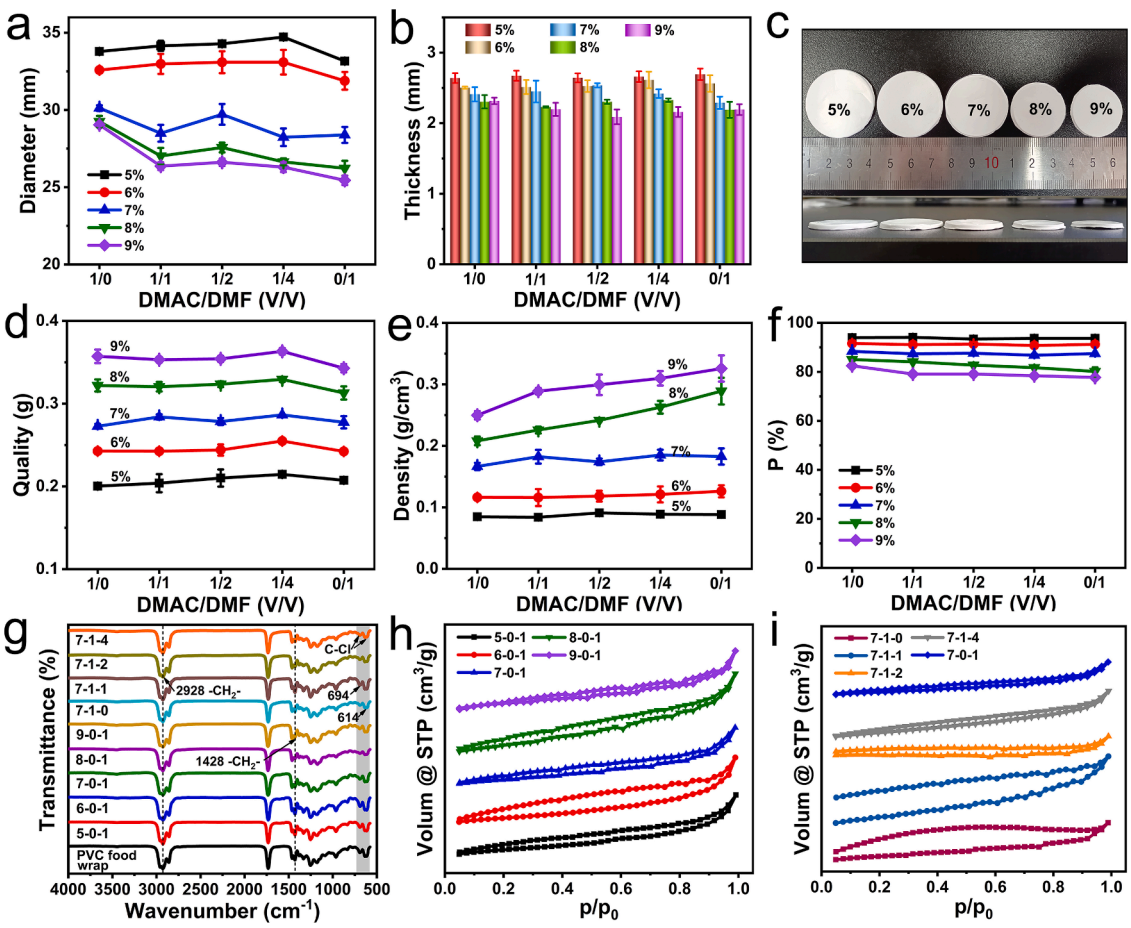

Fig. 2. The relationship between PVC sponges and solvent ratio and concentration. (a) diameter, (b) thickness, (c) photos, (d) quality, (e) density, (f) porosity, (g) FTIR spectra, (h) and (i) N_2 adsorption–desorption hysteresis curve.

prepared sponges indicate that higher solvent ratios and higher PVC concentrations lead to harder sponges. This phenomenon is attributed to its density and aligns with the results in Fig. 2e.

The FTIR spectra of PVC sponges are presented in Fig. 2g. The stretching and bending vibrations of $–CH_2-$ in PVC were observed at 2928 and 1428 cm^{-1}, respectively, while the telescopic vibrations of C-Cl were detected at 694 and 614 cm^{-1} [39]. The peak shapes of all PVC sponges were similar to those of the PVC food wrap, and no new characteristic peaks were observed. This suggests that the formation of PVC sponges involved physical dissolution, stacking, and recombination rather than a chemical reaction.

The N_2 adsorption–desorption curve of PVC sponges is shown in Fig. 2h and 2i. All PVC sponges exhibited typical type IV isotherms, indicating the presence of mesopores [40–42]. With increasing PVC concentration, the specific surface area of the sponges initially increased and then decreased, while the pore size displayed the opposite trend. The 8–0-1 had the highest specific surface area of 3.813 m^2/g (Fig. 2h). This may be due to the large interlayer spacing of sponges formed at low concentrations, resulting in a smaller surface area. Conversely, at high concentrations, the interlayer spacing was too small, causing the PVC microspheres to stack tightly and cover some of the surface areas inside the PVC, thereby reducing the specific surface area of the sponge.

However, the solvent had a significant impact on the specific surface area and pore volume of sponges (Fig. 2i). The 7–1-1 and 7–1-4 displayed relatively large specific surface areas and pore volumes because the solvent influences the crystallization and formation of PVC sponges, leading to different molecular arrangements. This result is consistent with the SEM images presented in Fig. 3, which depict irregularly arranged 7–1-1 and 7–1-4, exposing more specific surface area. The BJH pore size distribution plots and BET data for PVC sponges are presented in Fig. S2 and Table S1.

3.1. Morphology and structure analysis of PVC sponges

The microstructure of sponges is a crucial factor in determining their adsorption and separation properties. To analyze the microstructure of PVC sponges, SEM images were taken on both the surface and interior of the sponges. In the SEM images of the upper surface of PVC sponges (Fig. 3a), it is evident that the sponges are composed of microspheres of varying sizes and shapes, with rough surfaces that contribute to their unique surface property. Additionally, the concentration of PVC plays a significant role in determining the dispersion and aggregation of pellets on the sponges' surface. At higher concentrations of PVC, the spheres on the surface of the sponges tend to agglomerate and form larger blocks, resulting in the formation of multiple pellets clustered and wrapped aggregate blocks. The smaller the DMAC/DMF value, the easier it is for the pellets on the surface of the PVC sponges to aggregate into larger blocks.

SEM images (Fig. 3b) of the section of the sponges revealed a regular layered structure, with smaller and denser layer spacing observed at higher concentrations of PVC. When the PVC concentration reached 8 wt %, the layer spacing was very small, and the layers were tightly arranged, with no apparent layer structure visible. Moreover, the solvent used in the preparation process can also influence the layer arrangement, causing the PVC molecules to be arranged irregularly, as seen in Fig. 3b images of 7–1-1 and 7–1-4. It is plausible that the dissimilar solubility of DMAC and DMF in PVC food wrap may account for the observed phenomenon. By consulting the physical and chemical

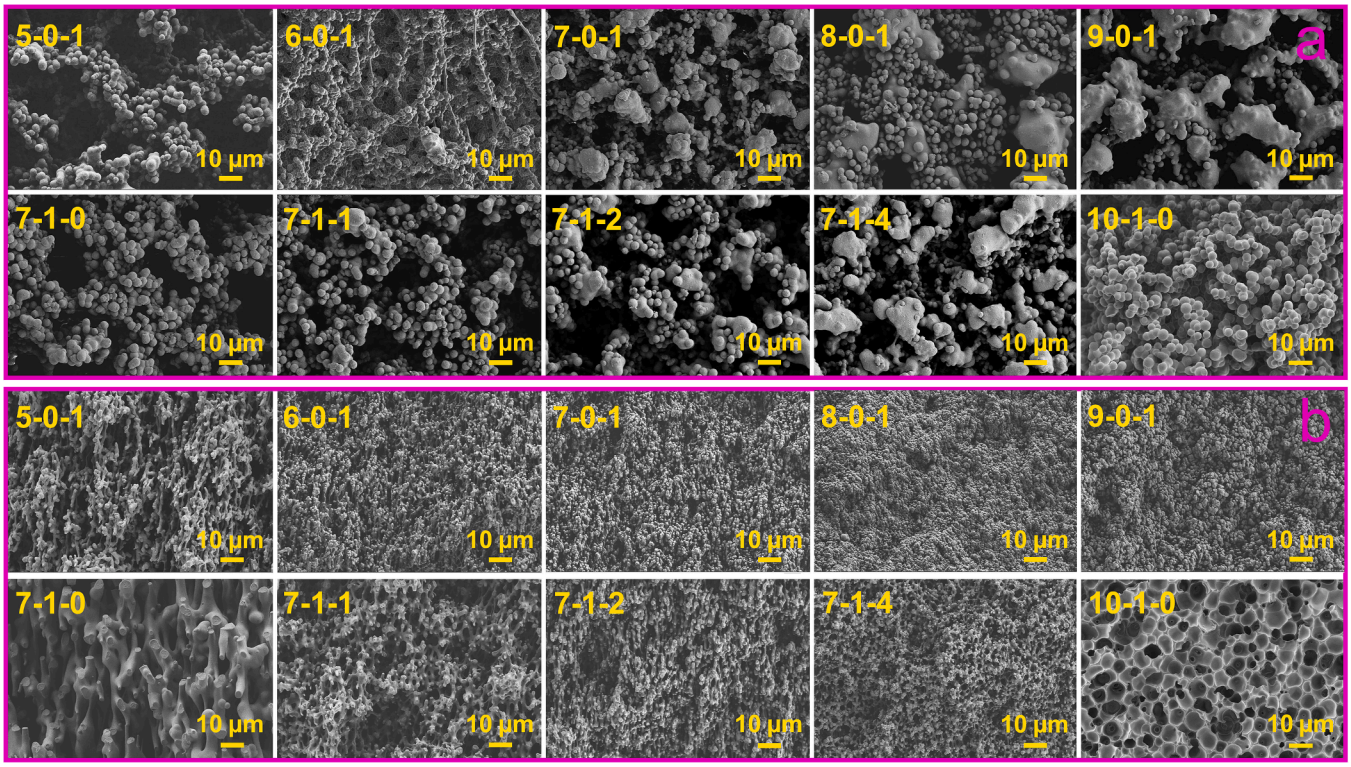

Fig. 3. The SEM images of (a) the upper surface and (b) the section of PVC sponges.

characteristics of these two solvents in Table S2, one can discern notable distinctions. Specifically, DMAC exhibits a greater molecular weight, higher viscosity and density, and a smaller solubility parameter. Adhering to the principles of similar miscibility and considering the solubility parameter of PVC to be 9.5 $(cal/cm^3)^{1/2}$, it becomes apparent that DMAC surpasses DMF in terms of solubility with PVC. Consequently, DMAC facilitates the dispersion of PVC molecules. Assuming the solvent solely comprises either DMAC or DMF. In such a scenario, the absence of steric effects from the other solvent allows the system to consist exclusively of a single solvent and PVC molecules. This enables the PVC molecules to disperse uniformly throughout the solvent, thereby resulting in a regular layered structure within the PVC sponge. Nevertheless, when both DMAC and DMF coexist within the solvent, a competitive relationship ensues as the two solvents vie for PVC molecules, driven by the interplay of solubility parameters and steric hindrance. DMAC, possessing superior solubility, a greater spatial ratio, and a more favorable affinity for PVC food wrap, may cause PVC molecules to gravitate towards it. This preference gives rise to an inherently less stable system wherein the dispersion of PVC molecules becomes uneven, ultimately leading to the formation of porous materials with an irregular arrangement of PVC. These unique features of the layered structure endow the sponges with exceptional compressibility and resilience. For the SEM images of sponges with a large doubling speed, please refer to supporting information Fig. S3.

We investigated the microstructure of the 10–1-0 that failed to pass through the w/o emulsion (Fig. 3). The upper surface of the 10–1-0 exhibits a relatively dense structure composed of microparticles of varying sizes. Meanwhile, its cross-section reveals a grid structure similar to hollow or solid spherical material links. The unique compact structure of the upper surface and the unconnected pore structure of the cross-section endow the 10–1-0 with unconnected properties. Under external force, the emulsion breaks upon contact with the sponge surface, and water droplets can adhere well to the sponge surface. However, due to the absence of network channels, oil droplets cannot be separated from the sponges. Consequently, we excluded the 10 wt% sponges from all subsequent experiments.

Morphologies of the sponges may differ depending on the different environments on the upper and lower surfaces, making SEM images on the lower surface essential to study the formation of its structural morphology. In Fig. 3, the morphology and arrangement of porous materials exhibit a profound interplay with their concentration. Evidently, the superficial characteristics of 5–0-1, 6–0-1, and 7-0-1 manifest striking dissimilarities. On the other hand, a comparative investigation of the SEM images captures a semblance between the upper surface of 8–0-1, 9–0-1, and 7-0-1, attained through the utilization of distinct solvents. Consequently, we elect to undertake a SEM analysis on the lower surface of 5–0-1 (depicted in Fig. 4a), 6–0-1 (depicted in Fig. 4b), and 7-0-1 (depicted in Fig. 4c). SEM images on three sponges with relatively different upper surface morphologies revealed that the structure of the lower surface of the three sponges is similar, with an intersected three-dimensional structure seen in all of them. Besides, the lower surface of the 10–1-0 features a planar structure with a pit structure, and consistent with the above results (Fig. 4d). However, the lower surface appears relatively smooth compared to the upper surface, as if it was pressed by a glass sheet, possibly because of its contact with the glass surface dish. Fig. 4e is a schematic diagram of the upper and lower surfaces of the sponge and with one side exposed to vapor designated as the upper surface, and the other side in contact with the surface dish designated as the lower surface.

The SEM results of the sponges demonstrate that the upper surface (Fig. 3a), section (Fig. 3b), and lower surface (Fig. 4) of PVC sponges are pore structures surrounded by microspheres, a layered structure, and pressurized network structure, respectively. This particular lamellar structure and surface structure is a result of its preparation method (vapor deposition). The hypothetical forming mechanism is as follows, building upon the understanding that PVC food wrap consists of a mixture of PVC molecules and plasticizers [43]. When PVC food wrap comes into contact with organic reagents, let's take dimethylformamide (DMF) as an example, the plasticizer within the PVC food wrap initially dissolves into the DMF solvent, creating an effective pathway for the

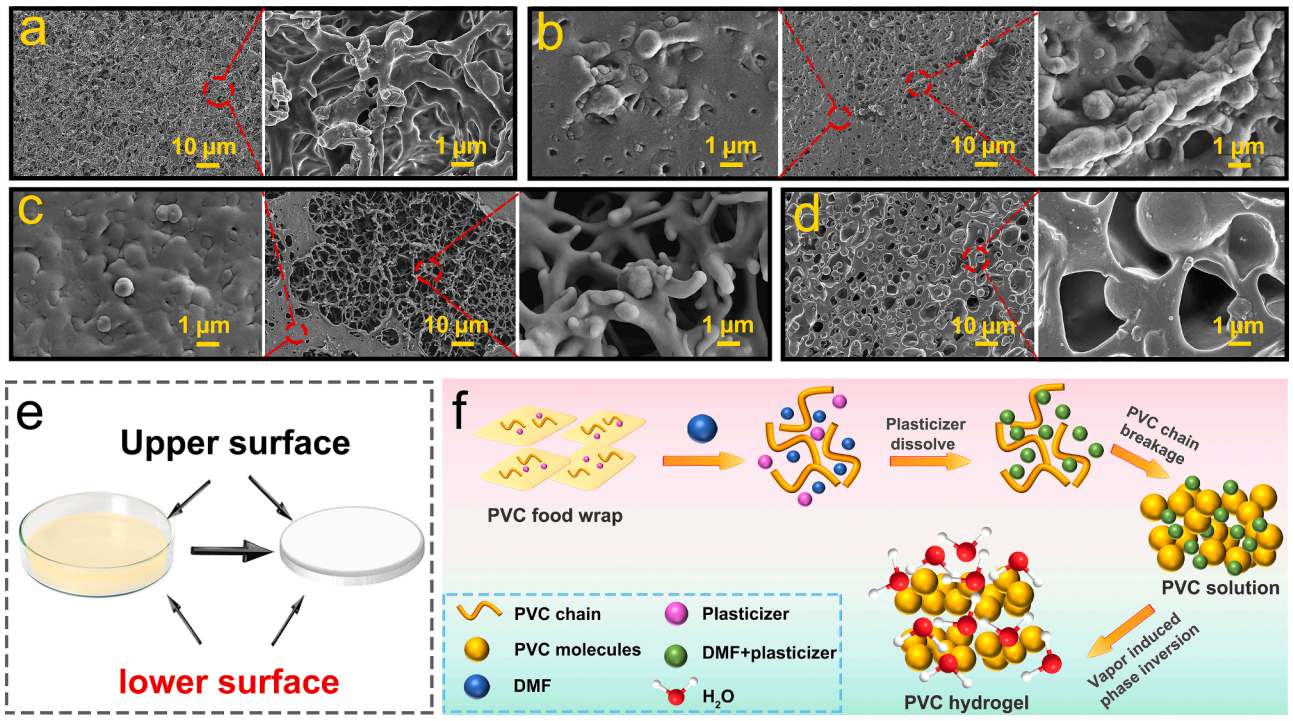

Fig. 4. The SEM images of the lower surface of (a) 5–0-1, (b) 6–0-1, (c) 7-0-1 and (d) 10–1-0; (e) The schematic diagram of surface indication of PVC sponges; (f) The schematic diagram of the formation of PVC sponge.

infiltration of DMF into the PVC molecules. Simultaneously, as the plasticizer content diminishes and the DMF content increases within the PVC food wrap, the spacing between PVC molecules expands, resulting in weakened interactions between PVC molecular chains. This weakening allows the PVC chains to fragment into multiple PVC molecules, which disperse uniformly within the DMF solvent as the dissolution time progresses.

Additionally, water is a bad solvent for PVC. Consequently, when PVC molecules in the solution come into contact with water molecules, PVC swiftly undergoes a phase transformation and precipitates out of the solution. Due to the even dispersion of PVC molecules in DMF, an abundance of water molecules exists on the upper surface of the PVC molecules during gas-induced phase transition technology. As water molecules move, the surface PVC molecules within the DMF solution come into contact primarily with the swifter and more numerous water vapor molecules. This phenomenon leads to the formation of clustered blocks on the upper surface of the PVC sponges.

Within the interior of the sponges, the larger volume of water vapor in the environment encounters resistance after the initial precipitation on the surface. Consequently, the smaller volume of water vapor in the environment can penetrate the PVC solution and establish contact with PVC molecules, thus resulting in a relatively uniform structure of PVC sponges. As water vapor gradually permeates the PVC solution from top to bottom, each layer within the PVC sponges acquires a comparable structure.

However, the bottom of the sponges interfaces with the glass surface, resulting in a smoothed lower surface. This process continues until all PVC molecules within the solution complete the phase conversion and precipitate, forming a hydrogel with a distinct layered structure comprised of multiple spherical compositions and stacks. The PVC sponge obtained through freeze-drying effectively preserves the original layered structure.

3.2. Thermal properties, rheological properties and processability of PVC sponges

The thermal properties, rheological properties and processability of the sponge are described in the supporting information.

3.3. Mechanical properties

To evaluate the mechanical properties of the sponges, we conducted bearing capacity and elastic properties tests on the 7-0-1 using the manual bearing weight method. As depicted in Fig. 5a, the rectangular-shaped 7-0-1 (length: 20 mm, width: 6 mm) was able to support a weight of 700 g without breaking even after being kept for 1 min. However, when an 800 g weight was applied, the sponge could only lift the weight off the table for a few seconds before breaking. Furthermore, as the weight increased, the sponge showed signs of elongation. These results suggest that the PVC sponges exhibit a remarkable load-bearing capacity and a certain degree of flexibility, with the ability to withstand a force of at least about 7 N.

Manual deformation experiments were performed to investigate the elastic properties of the sponge, and it was found that the sponges could be restored to their original shape after arbitrary extrusion deformation (Fig. 5b, videos 1 and 2). This indicates that the PVC sponges possess good flexibility and elastic recovery force, which allows them to adapt to the complex situations encountered in actual industrial applications. Moreover, the stress–strain plot of the sponges depicted in Fig. 5c reveals that the stress of the sponge increases with increasing PVC concentration, which may account for the observed increase in thickness and hardness of the sponge with increasing PVC concentration. Notably, the elongation at break of the PVC sponge is more than 100%, with an increase in PVC concentration leading to an increase in elongation at break except for 8–0-1, which exhibits a disordered structure that results in a larger distance between molecular chains and increased movement range of molecular chains. Consequently, the elongation at the break of 8–0-1 reaches 332%.

Furthermore, the stress–strain diagram of the sponges prepared from

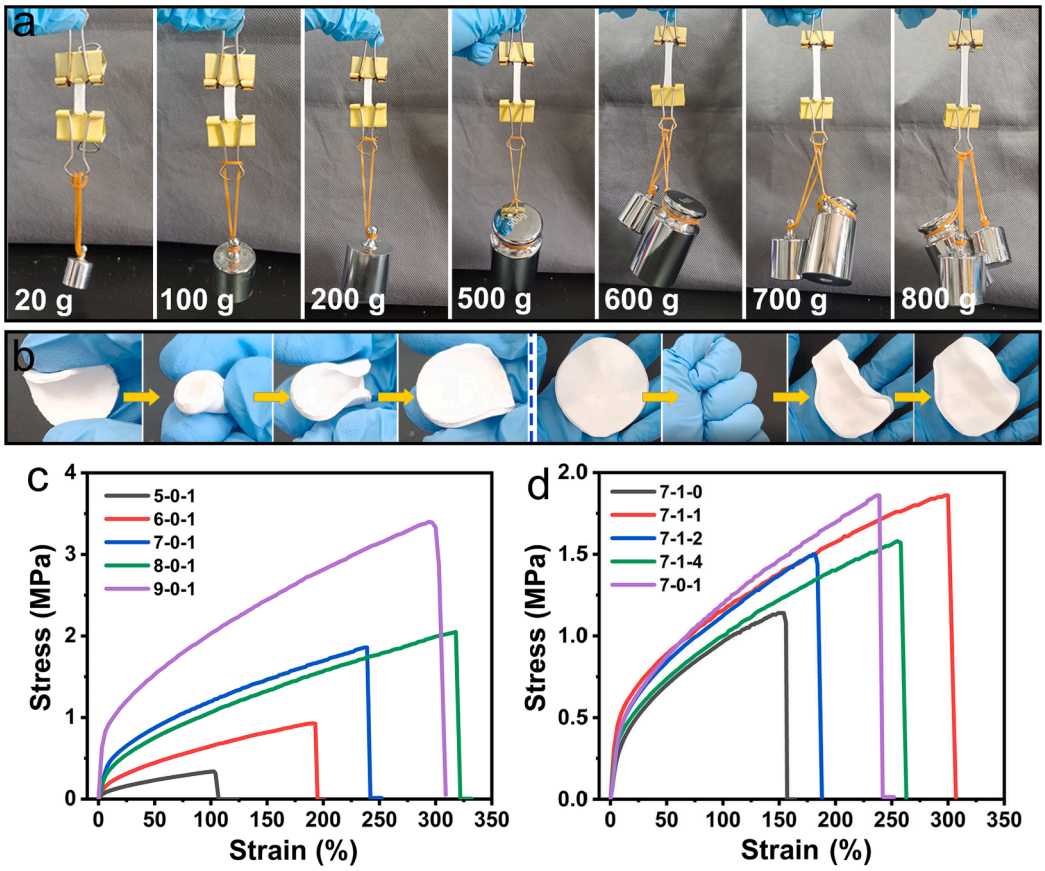

Fig. 5. (a) PVC sponges load bearing image; (b) Compression motion picture of PVC sponges; (c, d) Elastic stress–strain diagram of PVC sponges.

a 7 wt% PVC solution at different solvent ratios (Fig. 5d) revealed that the stress and elongation at break of the sponges do not show any significant regularity with an increase in DMAC/DMF ratio, which may be associated with the internal pore structure of the sponges (Fig. 3). Nevertheless, the elongation at break of the sponges remains at 150%. These findings indicate that PVC sponges possess excellent flexibility.

3.4. Effect of structure of PVC sponge on surface wettability and oil sorption properties

The surface wettability of the sponge was assessed by contact angle measurement. As shown in Fig. 6a, the PVC sponges exhibit remarkable wettability characteristics, with a contact angle of approximately 140°, which remains unaffected by the concentration of PVC and the ratio of DMAC/DMF. Fig. 6b demonstrates the ultra-lipophilicity (OCA = 0°) and hydrophobicity of the PVC sponges, with water droplets remaining on the surface of the sponge without significant alteration after 180 s, indicative of excellent hydrophobic stability. Furthermore, water droplets with acid, alkali, salt, and dye also maintain their droplet shape on the surface of the sponge, signifying their remarkable resistance to acid, alkali, and salt. This attribute expands the potential applications of the sponge in the environment. In addition, the sponge exhibits excellent plasticity, allowing it to be fabricated into various shapes, such as round sheets, cubes, flat bars, and pentagonal stars (Fig. 6c), rendering it highly versatile for practical applications.

The super-hydrophobic nature of the sponge affords it the ability to separate oil from water. As demonstrated in Fig. 6d, oil (n-hexane) stained with oil red is selectively adsorbed onto the sponge, while water stained with methylene blue remains unadsorbed, thereby enabling efficient separation of oil–water mixtures. Notably, n-hexane is rapidly sorption into the sponge within 1 s (Fig. 6e and video 3). The sorption capacity of n-hexane on sponges, fashioned under various preparation conditions, displays variation (see Fig. 6f). As the PVC concentration increases, the sorption capacity of the PVC sponges for n-hexane diminishes, while a minor decrease is observed with a decrease in the DMAC/DMF ratio. This finding is consistent with the outcomes obtained for the mass, pore density, and porosity of the PVC sponges. It thus becomes apparent that the oil sorption capacity of the PVC sponge is closely intertwined with its pore size and porosity. The sorption capacity for n-hexane decreases as the pore size diminishes, whereas it increases with an escalation in porosity. This arises from the fact that larger pore sizes in the sponge correspond to augmented effective pore volume, heightened porosity, amplified oil capacity, and consequently, an elevated oil sorption capacity. The sorption capacity of sponges fabricated with 5 wt% PVC concentration for n-hexane is the highest, at approximately 3 g/g. Higher concentrations of sponge result in increased mass and density, decreased interlayer spacing, and effective pore volume, leading to reduced sorption capacity.

Upon checking the adsorption of n-hexane through an assortment of plastic adsorbents, as concisely summarized in Table 1, one can readily observe that the adsorption potential of the PVC sponge, as explored in this investigation, rivals that of other plastic adsorbents documented in previous studies. Moreover, the raw materials employed in this undertaking exude a greener and simpler disposition, while the experimental protocol itself espouses an inclination towards simplicity and energy conservation. Moreover, the PVC sponge exhibits excellent recyclability and stability. For instance, the sorption capacity of 7-0-1 on n-hexane, cyclohexane, n-heptane, and petroleum ether remains stable even after 10 cycles (Fig. 6g). Remarkably, the hydrophobic angle and n-hexane sorption capacity of 7-0-1 prepared under copper sulfate, potassium chloride, and sodium chloride conditions do not vary, with values of approximately 140° and 1.5 g/g, respectively, indicating the universality of PVC sponges.

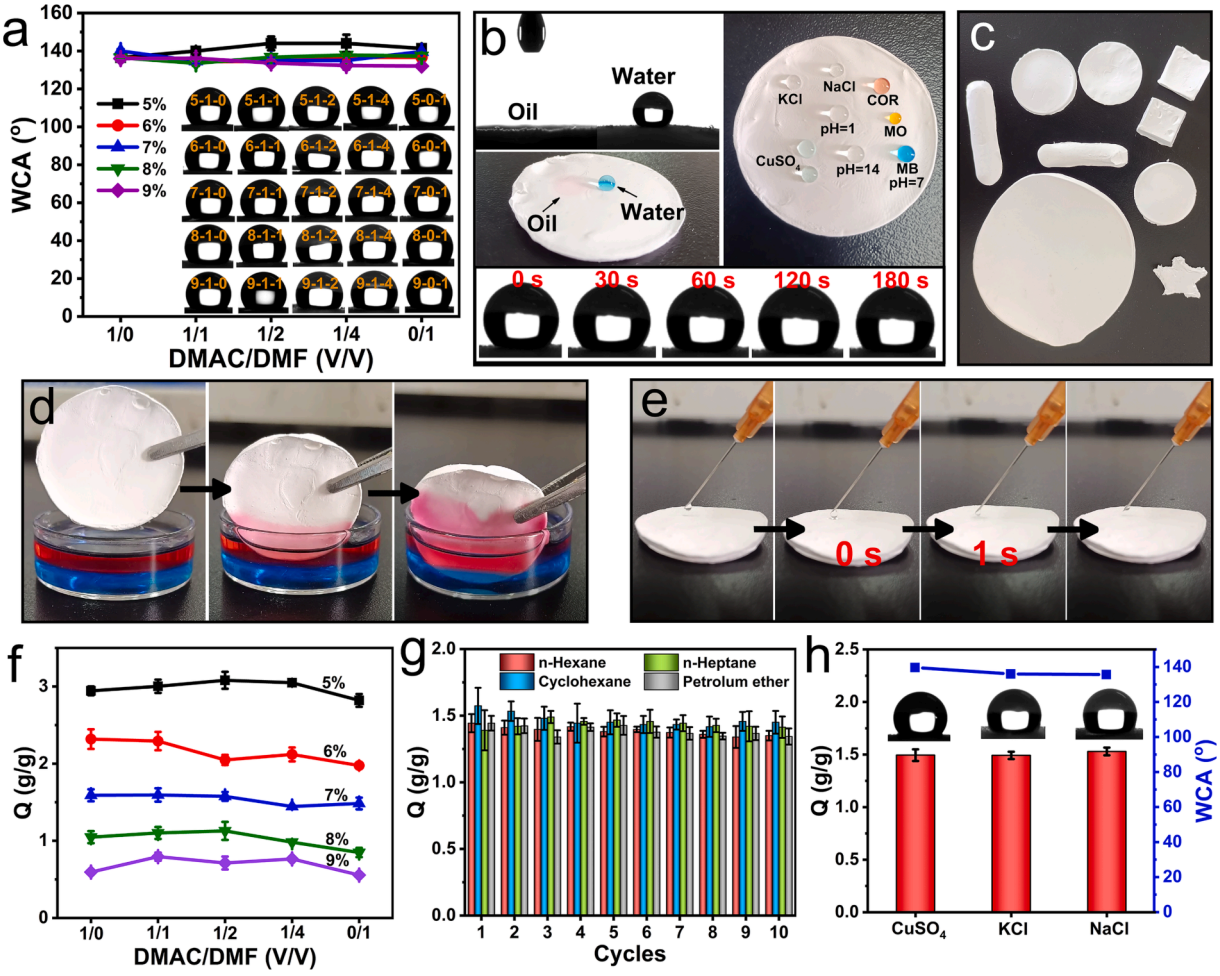

Fig. 6. (a) Water contact angle of PVC sponges; (b) Wettability of 7-0-1; (c) Flexibility of 7-0-1; (d) Dynamic diagram of oil–water separation of 7-0-1; (e) Oil sorption dynamic diagram of 7-0-1; (f) Sorption capacity diagram of PVC sponges for n-hexane; (g) Sorption cycle diagram of four kinds of oil on 7-0-1; (h) n-hexane sorption capacity and water contact angle of 7-0-1 prepared in three environments.

Table 1
The sorption of n-hexane on plastic-based materials.

Materials	Raw materials	Methods	Q (g/g)	Refs
MnO_2 nanowires/PU foam	Polyether polyol (NJ-330), hydrophobic MnO_2, KH 570, IPDI, $NaHCO_3$, silicone oil	Hydrothermal (100 °C, 3 h)	~7.5	[44]
PVDF aerogel	PVDF, DMSO	Vapor induced phase inversion (water vapor, 25 °C)	3.1	[34]
Porous CNT/PVDF	PVDF, CNT, DMF	Vapor induced phase inversion (methanol vapor, 3 days)	3.3	[45]
PC/cMWCNTs monolith	cMWCNT, PC granules, THF	Thermally induced phase separation (40 °C)	8.06	[46]
PP aerogels	PP granules, xylene	Thermally induced phase separation (80 °C)	~2.9	[47]
PS/PP monolith	PS, PP, ethanol	–	~7	[48]
Porous PLA film Flat PLA film	PLA (Mn = 69000), 1,4-dioxane, ethanol	Phase separation (ethanol)	~3.5 ~0.5	[49]
Shellac aerogel	Shellac, Na_2CO_3, gluconic acid lactone, trimethylsilyl chloride	Sol-gel (-10 °C, 24 h); chemical vapor deposition (40 °C, 24 h)	~3	[50]
PP/PTFE foams	PP pellets, PTFE powders	Twin-screw extrusion (100 ~ 200 °C); supercritical CO_2 foaming (180 °C)	~4.5	[51]
CNT/styrofoam	Commercial styrofoam, carbon nanofiber, acetone	Doping	3.38	[52]
PP/ZIF-8–1	PP non-woven fabric, 2-methylimidazole, $Zn(NO_3)_2{\cdot}6H_2O$, methanol	In-situ grown	~0.5	[53]
PVC sponge (5–1-2)	PVC food wrap, DMF, DMAC	Vapor induced phase inversion (water vapor, room temperature)	3.1	This work

Note: PU (polyurethane); IPDI (isophorone diisocyanate); PVDF (polyvinylidene fluoride); DMSO (dimethylsulfoxide); CNT (carbon nanotube); cMWCNT (carboxyl-functionalized multiwalled carbon nanotube); PC (polycarbonate); THF (tetrahydrofuran); PS (styrene monomer); PLA (polylactic acid); PP (polypropylene); PTFE (polytetrafluoroethylene).

3.5. Effect of structure of PVC sponge on emulsion separation performance properties

Fig. 7a presents a diagram illustrating the separation of water-in-n-hexane emulsions using PVC sponges. The results show that the emulsion flux of PVC sponges decreases as the concentration of PVC increases. Additionally, decreasing the DMAC/DMF ratio also results in a smaller emulsion flux. This is because the flux of emulsions passing through sponges is determined by their pore size and interlayer spacing. The smaller the pore size of the sponge, the longer the time required for the emulsion to pass through, resulting in a smaller flux. Similarly, the smaller the layer spacing of the sponge, the denser its pore structure, the greater the resistance of the liquid, and the longer the time required to pass through the sponge, leading to a smaller flux.

However, not all sponges can effectively separate emulsions. Only when the PVC concentration is high and the DMAC/DMF ratio is high (7-0-1, 8–1-2, 8–1-4, 8–0-1, 9–1-1, 9–1-2, 9–1-4, 9–0-1), can the sponges effectively separate the emulsions (Fig. 7c). After separation, the emulsion changed from turbidity to transparency. The size of water droplets in the emulsion before separation was mainly between 300–1000 nm, but it significantly decreased to a range of 3–6 nm after separation (Fig. 7b). These different separation and flux results of PVC sponges to emulsions may be caused by the three-dimensional lamellar structure inside the sponges. When the concentration of PVC is low, the sponge is relatively soft, and its internal pore structure and layer spacing are large. This macropore structure is larger than the size of water droplets in the emulsion, allowing the emulsion to quickly pass through the sponge under external force, resulting in a large flux. However, as the concentration of PVC increases, the inner layer structure of the sponge becomes more compact, making it more difficult for the emulsion to pass through the sponges, resulting in a decrease in its flux. Nonetheless, the macroporous structure is not improved, and the emulsion cannot be separated.

Only when the ratio of DMAC/DMF decreases and the internal

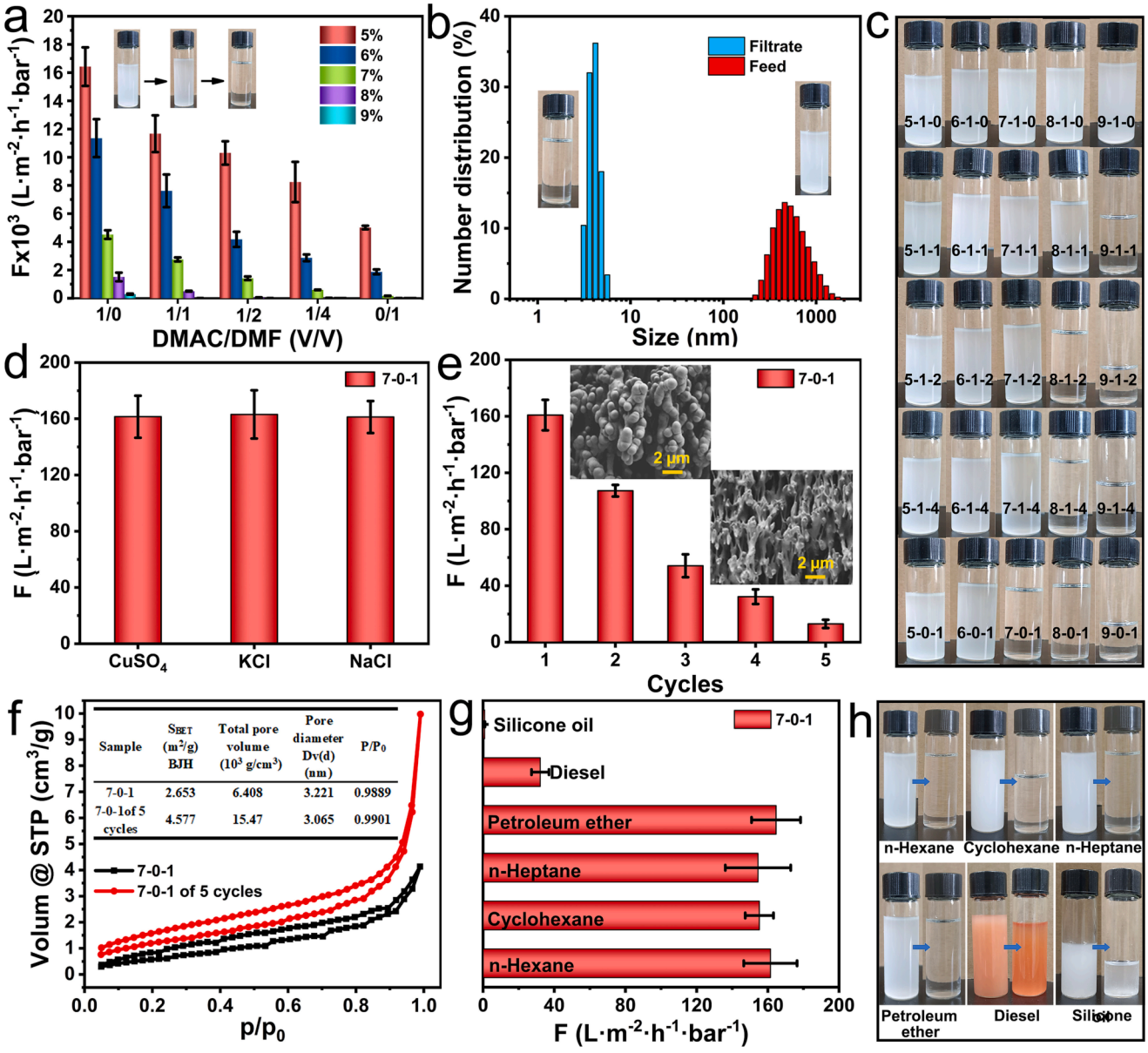

Fig. 7. (a) Flux of PVC sponges to 5 mL water/n-hexane emulsion; (b) Dimensions before and after 7-0-1 separation of the water/n-hexane emulsion; (c) The optical photo of PVC sponges after separation of the water/n-hexane emulsion; (d) Flux of 5 mL water/n-hexane emulsion of 7-0-1 prepared in three environments; (e) Circulation diagram of 7-0-1 separation emulsion (Inset are SEM of the section before and after five cycles of sponge); (f) BET plots of 7-0-1 before and after five cycles; (g) Flux of 7-0-1 to six w/o emulsions; (h) Comparison of optical photographs of 7-0-1 before and after separation of a w/o emulsion.

aperture of the sponge is reduced or the arrangement is irregular, can the sponge effectively separate the emulsion under the action of external force. In this way, oil can pass through, but water cannot, resulting in the separation of the emulsion. However, when the concentration is 9 wt% and the ratio of DMAC/DMF is reduced to 0/1, the emulsion finds it difficult to pass through the sponges, resulting in a very small emulsion flux. Therefore, the 7-0-1 was selected for the adsorption of other oils and performance testing of other emulsions.

The 7-0-1, prepared in the three different environments of copper sulfate, potassium chloride, and sodium chloride, exhibited excellent water-in-n-hexane emulsion separation capabilities, with fluxes exceeding 161.5 $L{\cdot}m^{-2}{\cdot}h^{-1}{\cdot}bar^{-1}$, as depicted in Fig. 7d. These results surpass those of reported emulsion separation materials. In comparing our PVC sponge with other separation materials, it is clear that the flux of emulsion cannot be easily equated. This flux is intricately linked to the thickness and wettability of the material [54]. Through our statistical investigation, we have observed that PVC-based materials are seldom employed in the separation of water-in-oil emulsions, and presently, we have come across no relevant reports on the matter. Simultaneously, when compared with other materials for n-hexane-in-water emulsions that have been reported (as shown in Table 2), the raw materials utilized in our PVC sponge exhibit simplicity and environmental friendliness. Furthermore, our sponge for water-in-hexane separation falls within a moderate range, surpassing certain water-in-oil materials. However, the cycle performance of the 7-0-1 sponge for emulsion separation was found to be poor (Fig. 7e). After the second cycle, the emulsion flux decreased by 55% from 161.5 $L{\cdot}m^{-2}{\cdot}h^{-1}{\cdot}bar^{-1}$ to 107.3 $L{\cdot}m^{-2}{\cdot}h^{-1}{\cdot}bar^{-1}$ in the first cycle. Furthermore, each subsequent cycle reduced by approximately half compared with the previous cycle until the fifth cycle, where the flux was only 12.9 $L{\cdot}m^{-2}{\cdot}h^{-1}{\cdot}bar^{-1}$.

To investigate the reason for the decline in emulsion flux, we compared the cross-section of the 7-0-1 before and after cycling five times. As shown in Fig. 7e and Fig. S6, the interlayer spacing of the sponge was noticeably reduced, and the density was increased after cycling five times, indicating that the sponge was compressed, and the resistance of the emulsion passing through the sponge was increased. The existence of the emulsifier may have contributed to the reduction in flux, as the tight layer structure may have made it difficult for the emulsion to demulsify, or the oil in the emulsion may have been unable to pass through, resulting in a significant decrease in the emulsion flux. The BET results of the sponge after five cycles (Fig. 7f and S7) showed that the specific surface area and pore volume increased to 4.577 m^2/g and 0.0155 cm^3/g, respectively, while the pore size decreased to 3.065 nm, indicating that the sponge was compressed.

In addition to its ability to separate w/o (n-hexane) emulsions, the 7-0-1 can also effectively separate other organic reagents and w/o emulsions, as demonstrated in Fig. 7g. The sponge exhibits varying separation fluxes for different types of emulsions, with superior performance observed for emulsions prepared with n-hexane, cyclohexane, petroleum ether, and n-heptane. Conversely, the sponge's separation efficiency for emulsions containing diesel and silicone oil is suboptimal, resulting in a lower flux. Remarkably, the 7-0-1 can even separate cloudy emulsions into transparent organic reagents and oil, as illustrated in Fig. 8h. This behavior can be attributed to the viscosity of the organic reagents and oils, as detailed in Table S4 of the supporting information. The viscosity of the oil affects the resistance of the formed emulsion to pass through the sponge and also influences its adherence to the sponge. Consequently, the 7-0-1 is particularly well-suited for separating w/o emulsions of organic reagents with lower viscosity. Overall, these results underscore the versatility of the 7-0-1 as a separation material for various types of organic reagents and w/o emulsions. Its unique properties and superior performance make it a promising candidate for a range of practical applications.

To provide a more comprehensive understanding of the impressive separation ability of the sponge, we employed optical microscopy to observe the emulsions prepared with four organic reagents, both before and after separation. As shown in Fig. 8a, the optical image displays distinct circles (water droplets) present in the n-hexane, cyclohexane, n-heptane, and petroleum ether emulsions before separation. However, the image captured after separation reveals no discernible circles, indicating that the separation efficiency of the sponges emulsion is remarkably high. Indeed, the sponges effectively remove water from the emulsion, yielding clean oil.

Based on these observations, we propose a plausible separation mechanism (as illustrated in Fig. 8b). The superior hydrophobicity and oil–water separation performance of the PVC sponges may be attributed to the presence of multiple hydrophobic -Cl groups along the PVC chain. Furthermore, the internal multi-layer network structure of the PVC sponges confers exceptional emulsion separation performance. When the external force is applied, the emulsion in contact with the surface of the sponge is driven downwards, causing demulsification to occur at the contact surface of a small aperture. Since the sponges' pore size is generally smaller than that of the water droplets, the water droplets become trapped on the surface and inside the sponge. In contrast, oil

Table 2
Comparison of preparation methods and water-in-n-hexane emulsion fluxes of different separation materials.

Materials	Raw materials	Methods	Flux	refs
PDA/PET/PVDF membrane	Coca bottles, PVDF, TFA, DCM, dopamine-HCl, ethylene diamine, DMF, acetone	Electrospinning; surface chemical modification	~2000 $L{\cdot}m^{-2}{\cdot}h^{-1}{\cdot}bar^{-1}$	[55]
PET@ZnO membrane	Cola bottles, TFA, DCM, $Zn(CH_3COO)_2{\cdot}2H_2O$,	Dual-solvent dissolution; electrospinning; in-situ growth	887 $L{\cdot}m^{-2}{\cdot}h^{-1}$	[56]
PVDF aerogel	PVDF, DMSO	Vapor induced phase inversion method (water vapor, 25 °C)	~ 225 $L{\cdot}m^{-2}{\cdot}h^{-1}$	[34]
PE aerogel membrane	Waste PE, hexadecane, ethanol, *tert*-butanol	Swelling (100 °C, 1 h; 135 °C, 4 h); solvent extraction	1726 $L{\cdot}m^{-2}{\cdot}h^{-1}$	[57]
Wood slice	Pine wood slice (1 mm), NaOH, $Cu(OH)_2$, dodecanethiol, ethanol	Vacuum impregnation; surface modification	8 $L{\cdot}m^{-2}{\cdot}h^{-1}$	[58]
Porous PVDF membrane	PVDF powder, citric acid monohydrate, DMF, $NaHCO_3$, ethanol	In-situ elimination	79.58 $L{\cdot}m^{-2}{\cdot}h^{-1}$	[59]
$Cu(OH)_2$ coated mesh	stainless steel meshes, acetone, ethanol, $CuCl_2$, NaOH, PU, n-dodecanethiol	Facile spraying; surface modification	~12.5 $L{\cdot}m^{-2}{\cdot}h^{-1}$	[60]
UIO-66-F4@rGO/filter paper membrane	TFTPA, $ZrCl_4$, FPSO, DBTDL, TEOS, acetone, glacial acetic acid, filter paper, methanol, GO, n-heptane	In-situ growth (110 °C, 24 h); cross-linking	549.29 $L{\cdot}m^{-2}{\cdot}h^{-1}$	[31]
ZnO/mesh	Stainless steel mesh, ZnO, ethanol, PU, stearic acid	Spraying; impregnation	~22 $L{\cdot}m^{-2}{\cdot}h^{-1}$	[61]
PVC sponge (7-0-1)	PVC food wrap, DMF	Vapor induced phase inversion (water vapor, room temperature)	161.5 $L{\cdot}m^{-2}{\cdot}h^{-1}{\cdot}bar^{-1}$	This work

Note: PDA (polydopamine); PET (polyethylene terephthalate); PVDF (polyvinylidene Fluoride); TFA (trifluoroacetic acid); PE (polyethylene); DCM (dichloromethane); PU (polyurethane); TFTPA (2,3,5,6-tetrafluoroterephthalic acid); DMSO (dimethylsulfoxide); FPSO (hydroxyl-fluoropolysiloxane); DBTDL (dibutyltin dilaurate); TEOS (tetraethoxysilane); GO (graphene oxide).

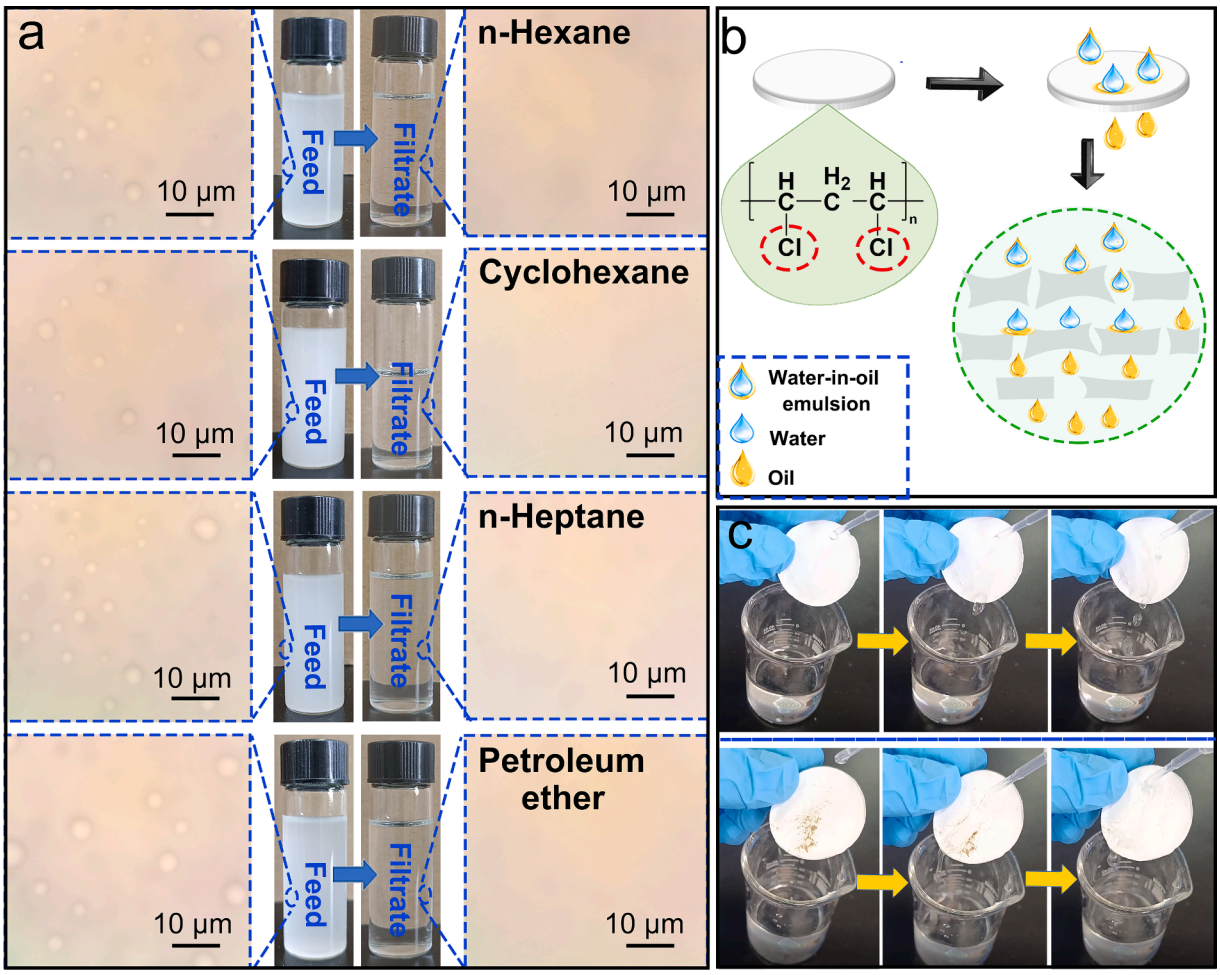

Fig. 8. (a) Micrographs before and after separation of four water-in-oil emulsions of n-hexane, cyclohexane, n-heptane and petroleum ether by 7-0-1; (b) Schematic diagram of separation of water-in-oil emulsion for PVC sponges separation; (c) Self-cleaning dynamic diagram of PVC sponges.

droplets can smoothly pass through the sponge, enabling efficient separation and recovery of the emulsion. Notably, our conclusion is consistent with the previously reported literature [34]. Moreover, the PVC sponge exhibits excellent self-cleaning properties. As illustrated in Fig. 8c, water droplets on the sponge surface can rapidly roll and slide, effectively removing any sand present on the sponge surface. This self-cleaning capability further underscores the potential of the PVC sponge as a promising material for oil–water separation applications.

3.6. Recyclability

In light of the strategic requirements for sustainable development and heightened environmental awareness, investigating the regenerative properties of sponges has gained significant importance. As illustrated in Fig. 9a, a PVC sponge can be regenerated with ease. Simply dissolving the used PVC sponge in DMAC and DMF solvents followed by vapor deposition and freeze-drying leads to the production of the regenerated sponge. This regenerated sponge exhibits excellent emulsion separation properties and avoids the risks of secondary pollution or alteration of the sponges' structure and characteristics.

Comparing the 7-0-1 to the recycled 7-0-1 obtained from the former's usage (Fig. 9b), we observed that the latter had a smaller diameter and thickness. This result could be due to the partial dissolution of auxiliary agents from the PVC food wrap into the mixed DMAC/DMF solvent. During water vapor-induced precipitation, these additional agents were not precipitated, leading to a smaller sponge size relative to the auxiliary agents. However, the recycled 7-0-1 was obtained from PVC sponge with fewer additional agents, causing the concentration of PVC in its solution to be relatively high, resulting in reduced volume size.

Furthermore, the infrared diagram peak shape of the recycled 7-0-1 was consistent with that of the 7-0-1 (Fig. 9c), indicating that the recycled 7-0-1 underwent no chemical structure change and was derived from the 7-0-1. These observations demonstrate the excellent regenerative properties of PVC sponges, thereby providing promising avenues for sustainable and environmentally conscious technological advancements. Upon analyzing the SEM images of the regenerated PVC sponge, a remarkable observation comes to light: the regenerated PVC sponge bears an uncanny resemblance to the specimen 7-0-1, showing an appearance characterized by a layered arrangement. Such findings are captured in Fig. 9d, e, and f.

The recycled 7-0-1 exhibited a larger pore radius and porosity than the 7-0-1, with a smaller specific surface area and pore volume of 2.038 m^2/g and 0.004613 cm^3/g, respectively (Fig. 9g). The pore size distribution is presented in Fig. S8, which is consistent with the findings obtained for PVC sponges. Furthermore, the recycled 7-0-1 showed similar sorption and separation cycling capacity for n-hexane and w/o emulsions, as observed for the 7-0-1.

The recycled sponges perform similarly to PVC, exhibiting superior oil/water separation and emulsion separation performance, and cycle regeneration performance (Fig. 9h and 9i). With readily available raw materials and simple preparation methods, PVC sponge has the potential to be produced on an industrial scale and utilized in various separation applications of oily wastewater and w/o emulsions.

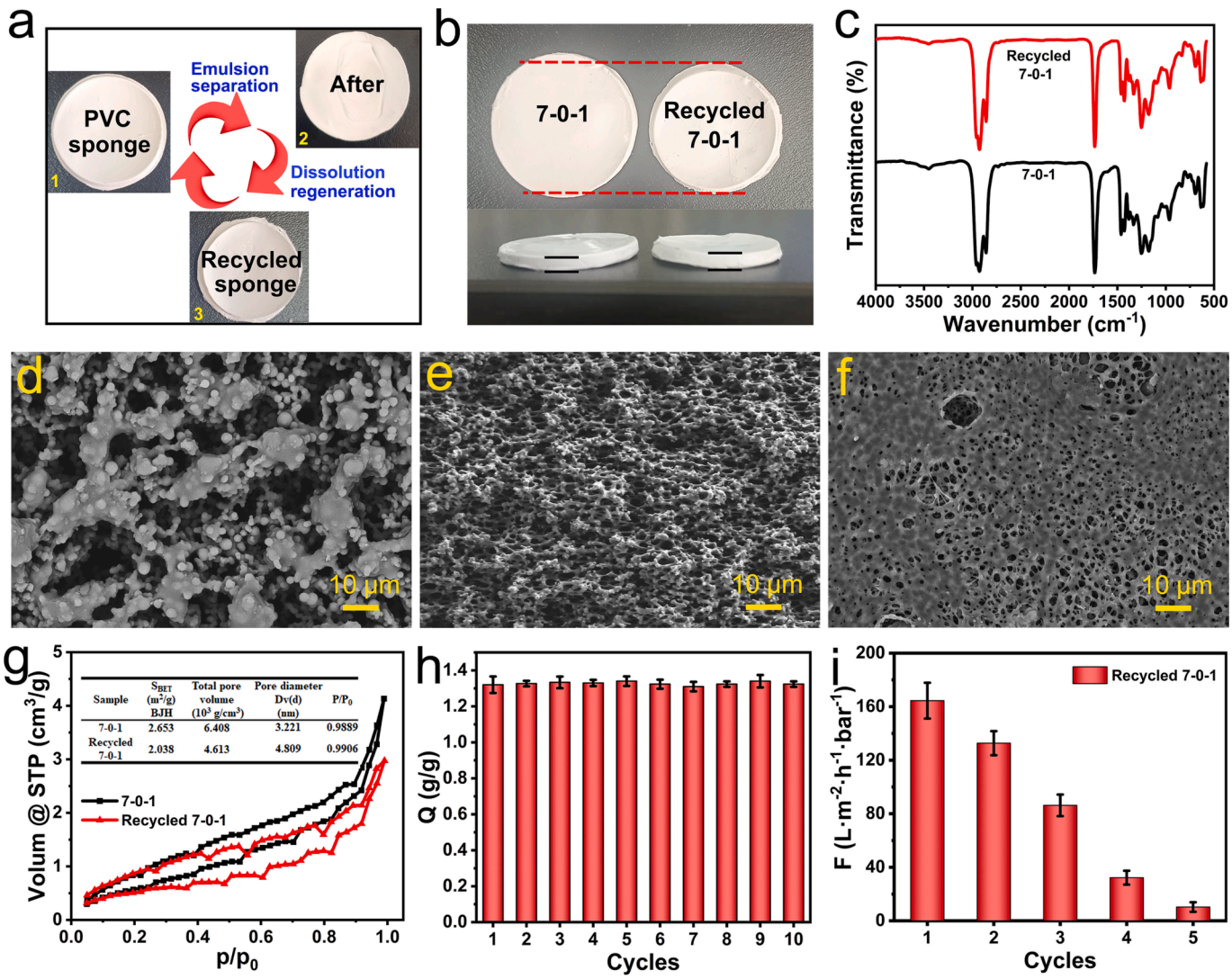

Fig. 9. (a) Diagram of a recycling process from a waste sponge to a new sponge: (1) The optical image of PVC sponge. (2) The optical image of PVC sponge after emulsion separation. (3) The optical image of recycled sponge obtained by dissolving mixed solution of DMAC and DMF, vapor deposition and freeze-drying; (b) Comparison of pictures before and after PVC sponge regeneration; (c) The FTIR image of PVC sponge and recycled 7-0-1; The SEM images of (d) the upper, (e) the section and (f) the lower surface of recycled 7-0-1; (h) The BET plots of PVC sponge and recycled 7-0-1; (i) n-hexane sorption cycle diagram of recycled 7-0-1; (g) Water-in-n-hexane emulsion flux cycle diagram for recycled 7-0-1.

4. Conclusion

This investigation presents a novel method for the synthesis of PVC sponge material with a distinctive layered structure and internal pores using recycled PVC food wrap. The oil–water separation and emulsion separation performance of the sponge material were evaluated, with excellent results. The sponges' layered structure was achieved through vapor deposition, while the PVC concentration and solvent determined the sponge's compactness. The sponges' ability to effectively separate oil from emulsified oil is attributed to the interaction between internal pore size and stratification. The emulsion separation of the PVC sponge was found to be clearer, and the flux smaller, with higher concentrations of PVC and lower DMAC/DMF values. Specifically, when the PVC concentration was 7 wt% and DMAC/DMF = 0/1, the sponge demonstrated superior emulsion separation performance. Due to the inherent properties of the PVC food wrap, the PVC sponge exhibited excellent elastic resilience, hydrophobicity, oil–water separation performance, and oil sorption stability. Remarkably, even after the second dissolution, vapor deposition, and freeze-drying process, the recycled sponge maintained good hydrophobicity, oil absorption stability, and emulsion separation performance. The preparation of this sponges material presents a promising solution to alleviate the pollution caused by PVC plastics, and provides an effective means for the efficient utilization of resources and energy, promoting sustainable development.

Declaration of Competing Interest

The authors declare that they have no known competing financial interests or personal relationships that could have appeared to influence the work reported in this paper.

Data availability

No data was used for the research described in the article.

Acknowledgements

We acknowledge the financial support provided by the Outstanding Youth Foundation of Xinjiang Autonomous Region, the Graduate Research Innovation Project of Xinjiang Uyghur Autonomous Region

(No. XJ2023G038), the National Natural Science Foundation of China (No. 21868036 and No. 32061133005), the Open Project Program of Key Laboratory of Xinjiang Uygur Autonomous Region (No. 2022D04012), the Outstanding Young Science and Technology Talents Project of Tianshan Youth Plan in Xinjiang Uygur Autonomous Region (No. 2020Q011 and No. 2020Q013). We would like to thank Shiyanjia Lab (https://www.shiyanjia.com) for SEM, TG and BET measurements.

Appendix A. Supplementary data

Supplementary data to this article can be found online at https://doi.org/10.1016/j.cej.2023.144752.

References

[1] A. Al Shami, G. Harik, I. Alameddine, D. Bruschi, D.A. Garcia, M. El-Fadel, Risk assessment of oil spills along the Mediterranean coast: A sensitivity analysis of the choice of hazard quantification, Sci. Total Environ. 574 (2017) 234–245.
[2] S. Liubartseva, M. De Dominicis, P. Oddo, G. Coppini, N. Pinardi, N. Greggio, Oil spill hazard from dispersal of oil along shipping lanes in the Southern Adriatic and Northern Ionian Seas, Mar. Pollut. Bull. 90 (1-2) (2015) 259–272.
[3] T. Zhang, Z. Li, Y. Lü, Y.u. Liu, D. Yang, Q. Li, F. Qiu, Recent progress and future prospects of oil-absorbing materials, Chin. J. Chem. Eng. 27 (6) (2019) 1282–1295.
[4] Y. Li, G. Zhang, A. Gao, J. Cui, S. Zhao, Y. Yan, Robust graphene/poly(vinyl alcohol) janus aerogels with a hierarchical architecture for highly efficient switchable separation of oil/water emulsions, ACS Appl. Mater. Inter. 11 (40) (2019) 36638–36648.
[5] S. Yang, L. Chen, S. Liu, W. Hou, J. Zhu, Q. Zhang, P. Zhao, Robust bifunctional compressed carbon foam for highly effective oil/water emulsion separation, ACS Appl. Mater. Inter. 12 (40) (2020) 44952–44960.
[6] Y. Huang, T. Gancheva, B.D. Favis, A. Abidli, J. Wang, C.B. Park, Hydrophobic porous polypropylene with hierarchical structures for ultrafast and highly selective oil/water separation, ACS Appl. Mater. Interfaces 13 (14) (2021) 16859–16868.
[7] Y. Guan, D. Qiao, L. Dong, X. Chen, Z. Wang, Y. Li, Efficient recovery of highly viscous crude oil spill by superhydrophobic ocean biomass-based aerogel assisted with solar energy, Chem. Eng. J. 467 (2023), 143532.
[8] O.A. Tafreshi, S. Ghaffari-Mosanenzadeh, Z. Ben Rejeb, Z. Saadatnia, M. M. Rastegardoost, C. Zhang, C.B. Park, H.E. Naguib, Amphiphilic polyimide-graphene nanoplatelet aerogel composites with high mechanical stability and enhanced thermal insulation properties for oil sorption applications, Materials Today Sustainability 22 (2023), 100403.
[9] B. Wang, R. Zheng, K. Shi, X. Ji, Evaluation of intrinsic-type and hydrophobic three-dimensional melamine/polyvinyl-alcohol formaldehyde sponges containing a hierarchical porous structure for emulsion separation, ACS Appl. Polym. Mater. 5 (1) (2023) 923–934.
[10] M.H. Tai, B.C. Mohan, C.-H. Wang, Freeze-casting multicomponent aerogel membrane with controllable asymmetric multilayer configuration for high flux gravity-driven separation of oil-water emulsion, Sep. Purif. Technol. 293 (2022), 121087.
[11] M. Zhu, Y. Liu, M. Chen, Z. Xu, L. Li, Y. Zhou, Metal mesh-based special wettability materials for oil-water separation: A review of the recent development, J. Petrol. Sci. Eng. 205 (2021), 108889.
[12] X. Yue, D. Fu, T. Zhang, D. Yang, F. Qiu, Superhydrophobic stainless-steel mesh with excellent electrothermal properties for efficient separation of highly viscous water-in-crude oil emulsions, Ind. Eng. Chem. Res. 59 (40) (2020) 17918–17926.
[13] W. Ma, Y. Li, S. Gao, J. Cui, Q. Qu, Y. Wang, C. Huang, G. Fu, Self-healing and superwettable nanofibrous membranes with excellent stability toward multifunctional applications in water purification, ACS Appl. Mater. Inter. 12 (20) (2020) 23644–23654.
[14] Y. Lu, D. Wu, Y. Qin, Y. Xie, Y. Ling, H. Ye, Y. Zhang, Facile construction of BiOBr/CoAl-LDH heterojunctions with suppressed Z-axis growth for efficient photoreduction of CO_2, Sep. Purif. Technol. 302 (2022), 122090.
[15] Y. Zhang, Y. Wang, C. Guo, Y. Wang, Molybdenum carbide-based photocatalysts: Synthesis, functionalization, and applications, Langmuir 38 (2022) 12739–12756.
[16] H. Wang, W. Zou, C. Liu, Y. Sun, Y. Xu, W. Sun, Y. Wang, β-Ketoenamine-linked covalent organic framework with Co intercalation: Improved lithium-storage properties and mechanism for high-performance lithium-organic batteries, Batteries Supercaps 6 (2023) e202200434.
[17] J. Wang, H. Wang, Ultra-hydrophobic and mesoporous silica aerogel membranes for efficient separation of surfactant-stabilized water-in-oil emulsion separation, Sep. Purif. Technol. 212 (2019) 597–604.
[18] S. Wang, Z. Wen, S. Shi, W. Hou, Preparation and oil absorption performance of polyacrylonitrile / reduced graphene oxide composite porous material, J. Water Process Eng. 41 (2021), 102092.
[19] C. Chen, C. Li, D. Yu, M. Wu, A facile method to prepare superhydrophobic nanocellulose-based aerogel with high thermal insulation performance via a two-step impregnation process, Cellul. 29 (1) (2022) 245–257.
[20] M.V. Lorevice, E.O. Mendonça, N.M. Orra, A.C. Borges, R.F. Gouveia, Porous cellulose nanofibril–natural rubber latex composite foams for oil and organic solvent absorption, ACS Appl. Nano Mater. 3 (11) (2020) 10954–10965.
[21] W. Li, W.-L. Jin, H.-X. Jiang, R. Wang, H. Jia, J.-Q. Liu, A.-N. Tang, L.-N. Zhu, D.-M. Kong, Facile fabrication of hierarchically porous melamine foam@COF composite for sample treatment of non-targeted food safety analysis and oil/water separation, Chem. Eng. J. 455 (2023), 140900.
[22] N. Xue, H. Cui, W. Dong, W. Chu, M. Li, H. Jiang, N. Wei, Multifunctional hydrophilic MXene/Gelatin composite aerogel with vertically aligned channels for efficient sustainable solar water evaporation and Oil/Water separation, Chem. Eng. J. 455 (2023), 140614.
[23] R.R. Bora, R. Wang, F. You, Waste polypropylene plastic recycling toward climate change mitigation and circular economy: Energy, environmental, and technoeconomic perspectives, ACS Sustain. Chem. Eng. 8 (2020) 16350–16363.
[24] S. Marullo, C. Rizzo, N.T. Dintcheva, F. D'Anna, Amino acid-based cholinium ionic liquids as sustainable catalysts for PET depolymerization, ACS Sustain. Chem. Eng. 9 (45) (2021) 15157–15165.
[25] V. Najafi, H. Abdollahi, Internally plasticized PVC by four different green plasticizer compounds, Eur. Polym. J. 128 (2020), 109620.
[26] M. Hasan, M. Lee, Enhancement of the thermo-mechanical properties and efficacy of mixing technique in the preparation of graphene/PVC nanocomposites compared to carbon nanotubes/PVC, Prog. Nat. Sci-Mater. 24 (6) (2014) 579–587.
[27] Q. Yang, Y. Xia, D. Zhang, X. Wang, S. Oliver, X. Chen, S. Shi, L. Lei, One-pot polyvinyl chloride preparation utilizing polyacrylate latex with tertiary amine groups for improved thermal stability, toughness, and reduced reactor scaling, Polym. Test. 90 (2020), 106691.
[28] X.-Y. Bai, Q.-W. Wang, S.-J. Sui, C.-S. Zhang, The effects of wood-flour on combustion and thermal degradation behaviors of PVC in wood-flour/poly(vinyl chloride) composites, J. Anal. Appl. Pyrol. 91 (1) (2011) 34–39.
[29] A. Abidli, Y. Huang, P. Cherukupally, A.M. Bilton, C.B. Park, Novel separator skimmer for oil spill cleanup and oily wastewater treatment: From conceptual system design to the first pilot-scale prototype development, Environ. Technol. Innov. 18 (2020), 100598.
[30] C. Chen, D. Weng, A. Mahmood, S. Chen, J. Wang, Separation mechanism and construction of surfaces with special wettability for oil/water separation, ACS Appl. Mater. Inter. 11 (11) (2019) 11006–11027.
[31] Y. Zhan, S. He, J. Hu, S. Zhao, G. Zeng, M. Zhou, G. Zhang, A. Sengupta, Robust super-hydrophobic/super-oleophilic sandwich-like UIO-66-F4@rGO composites for efficient and multitasking oil/water separation applications, J. Hazard. Mater. 388 (2020), 121752.
[32] M. Wu, P. Mu, B. Li, Q. Wang, Y. Yang, J. Li, Pine powders-coated PVDF multifunctional membrane for highly efficient switchable oil/water emulsions separation and dyes adsorption, Sep. Purif. Technol. 248 (2020), 117028.
[33] W. Deng, M. Long, Q. Zhou, N. Wen, W. Deng, One-step preparation of superhydrophobic acrylonitrile-butadiene-styrene copolymer coating for ultrafast separation of water-in-oil emulsions, J. Colloid Interf. Sci. 511 (2018) 21–26.
[34] X. Chen, Y.N. Liang, X.-Z. Tang, W. Shen, X. Hu, Additive-free poly (vinylidene fluoride) aerogel for oil/water separation and rapid oil absorption, Chem. Eng. J. 308 (2017) 18–26.
[35] Y. Yang, X. Chen, Y. Li, Z. Yin, M. Bao, Construction of a superhydrophobic sodium alginate aerogel for efficient oil Absorption and emulsion separation, Langmuir 37 (2) (2021) 882–893.
[36] Y. Janqamsari, M. Ashjari, Z. Niazi, Carbon nanotube promoted porous nanocomposite based on PVA and recycled PET fibers for efficient oil spills cleanup applications, Chem. Pap. 75 (7) (2021) 3443–3456.
[37] J.P. Chaudhary, N. Vadodariya, S.K. Nataraj, R. Meena, Chitosan-based aerogel membrane for robust oil-in-water emulsion separation, ACS Appl. Mater. Inter. 7 (44) (2015) 24957–24962.
[38] J. Wu, H. Li, X. Lai, Z. Chen, X. Zeng, Superhydrophobic polydimethylsiloxane@ multiwalled carbon nanotubes membrane for effective water-in-oil emulsions separation and quick deicing, Ind. Eng. Chem. Res. 58 (20) (2019) 8791–8799.
[39] E. Yousif, D.S. Ahmed, A.A. Ahmed, A.S. Hameed, S.H. Muhamed, R.M. Yusop, R. Amamer, S.A. Mohammed, The effect of high UV radiation exposure environment on the novel PVC polymers, Environ. Sci. Pollut. R. 26 (2019) 9945–9954.
[40] X. Chen, J. Cui, X. Xu, B. Sun, L. Zhang, W. Dong, C. Chen, D. Sun, Bacterial cellulose/attapulgite magnetic composites as an efficient adsorbent for heavy metal ions and dye treatment, Carbohyd. polym. 229 (2020), 115512.
[41] B. Zhao, L. Ren, Y. Du, J. Wang, Eco-friendly separation layers based on waste peanut shell for gravity-driven water-in-oil emulsion separation, J. Clean. Prod. 255 (2020), 120184.
[42] B. Qin, Y. Li, H. Kang, S. Huang, Q.i. Xiao, Tailoring pore structures and hydrophobicity of monolithic carbon nanofiber aerogels for optimized adsorption performance, J. Mater. Sci. 57 (5) (2022) 3211–3221.
[43] X. Zhang, C. Zhang, J.M. Hankett, Z. Chen, Molecular surface structural changes of plasticized PVC materials after plasma treatment, Langmuir 29 (12) (2013) 4008–4018.
[44] T. Zhang, L. Kong, Y. Dai, X. Yue, J. Rong, F. Qiu, J. Pan, Jianming Pan a, b,⇑, Enhanced oils and organic solvents absorption by polyurethane foams composites modified with Mn_O2 nanowires, Chem. Eng. J. 309 (2017) 7–14.
[45] Y. Yu, H. Chen, Y. Liu, V.S.J. Craig, L.H. Li, Y. Chen, A. Tricoli, Porous carbon nanotube/polyvinylidene fluoride composite material: Superhydrophobicity/superoleophilicity and tunability of electrical conductivity, Polymer 55 (2014) 5616–5622.
[46] Z. Li, B.o. Wang, X. Qin, Y. Wang, C. Liu, Q. Shao, N. Wang, J. Zhang, Z. Wang, C. Shen, Z. Guo, Superhydrophobic/superoleophilic polycarbonate/carbon nanotubes porous monolith for selective oil adsorption from water, ACS Sustain. Chem. Eng. 6 (11) (2018) 13747–13755.
[47] X.H. Lang, T.Y. Zhu, L. Zou, K. Prakashan, Z.X. Zhang, Fabrication and characterization of polypropylene aerogel material and aerogel coated hybrid

materials for oil-water separation applications, Prog. Org. Coat. 137 (2019), 105370.
[48] N. Baig, T.A. Saleh, Novel hydrophobic macroporous polypropylene monoliths for efficient separation of hydrocarbons, Compos. B: Eng. 173 (2019), 106805.
[49] Z. Xue, Z. Sun, Y. Cao, Y. Chen, L. Tao, K. Li, L. Feng, Q. Fu, Y. Wei, Superoleophilic and superhydrophobic biodegradable material with porous structures for oil absorption and oil–water separation, RSC Adv. 3 (2013) 23432.
[50] K. Li, Q. Luo, J. Xu, K. Li, W. Zhang, L. Liu, J. Ma, H. Zhang, A novel freeze-drying-free strategy to fabricate a biobased tough aerogel for separation of oil/water mixtures, J. Agric. Food Chem. 68 (12) (2020) 3779–3785.
[51] H.-Y. Mi, X. Jing, Y. Liu, L. Li, H. Li, X.-F. Peng, H. Zhou, Highly durable superhydrophobic polymer foams fabricated by extrusion and supercritical CO(2) foaming for selective oil absorption, ACS Appl. Mater. Inter. 11 (7) (2019) 7479–7487.
[52] N. Baig, F.I. Alghunaimi, T.A. Saleh, Hydrophobic and oleophilic carbon nanofiber impregnated styrofoam for oil and water separation: A green technology, Chem. Eng. J. 360 (2019) 1613–1622.
[53] X. Yang, S. Li, Y. Yao, J. Zhao, Z. Zhu, C. Chai, Preparation and characterization of polypropylene non-woven fabric/ZIF-8 composite film for efficient oil/water separation, Polym. Test. 100 (2021), 107263.
[54] Q. Tian, F. Qiu, Z. Li, Q. Xiong, B. Zhao, T. Zhang, Structured sludge derived multifunctional layer for simultaneous separation of oil/water emulsions and anions contaminants, J. Hazard. Mater. 432 (2022), 128651.
[55] Q. Xiong, H. Chen, Q. Tian, X. Yue, F. Qiu, T. Zhang, A.-B. Wang, Waste PET derived Janus fibrous membrane for efficient oil/water emulsions separation, J. Environ. Chem. Eng. 10 (2022), 108459.
[56] Q.i. Xiong, Q. Tian, X. Yue, J. Xu, X.u. He, F. Qiu, T. Zhang, Superhydrophobic PET@ZnO nanofibrous membrane extract from waste plastic for efficient water-in-oil emulsion separation, Ind. Eng. Chem. Res. 61 (32) (2022) 11804–11814.
[57] L. Gan, D. Zhang, X. Yue, J. Xu, F. Qiu, T. Zhang, A recyclable and regenerated aerogel membrane derived from waste plastic for emulsion separation, J. Environ. Chem. Eng. 10 (2022), 108221.
[58] X. Bai, Y. Shen, H. Tian, Y. Yang, H. Feng, J. Li, Facile fabrication of superhydrophobic wood slice for effective water-in-oil emulsion separation, Sep. Purif. Technol. 210 (2019) 402–408.
[59] L. Chen, Y. Si, H. Zhu, T. Jiang, Z. Guo, A study on the fabrication of porous PVDF membranes by in-situ elimination and their applications in separating oil/water mixtures and nano-emulsions, J Membrane Sci. 520 (2016) 760–768.
[60] X. Yin, Z. Wang, Y. Shen, P. Mu, G. Zhu, J. Li, Facile fabrication of superhydrophobic copper hydroxide coated mesh for effective separation of water-in-oil emulsions, Sep. Purif. Technol. 230 (2020), 115856.
[61] X. Bai, Z. Zhao, H. Yang, J. Li, ZnO nanoparticles coated mesh with switchable wettability for on-demand ultrafast separation of emulsified oil/water mixtures, Sep. Purif. Technol. 221 (2019) 294–302.